Journal of Materials Chemistry B

Accepted Manuscript

This article can be cited before page numbers have been issued, to do this please use: S. Patra, T. Hidalgo-Crespo, A. Permyakova, C. Sicard, C. Serre, A. Chausse, N. Steunou and L. Legrand, *J. Mater. Chem. B*, 2015, DOI: 10.1039/C5TB01412C.

ROYAL SOCIETY OF CHEMISTRY

www.rsc.org/materialsB

View Article Online
DOI: 10.1039/C5TB01412C

Journal Name

ARTICLE

Design of Metal Organic Frameworks-enzymes based bioelectrodes as novel and highly sensitive biosensing platform. †

Received 00th January 20xx,
Accepted 00th January 20xx

DOI: 10.1039/x0xx00000x

www.rsc.org/

Snehangshu Patra,[abc] Tania Hidalgo Crespo,[c] Anastasia Permyakova,[c] Clémence Sicard,[c] Christian Serre,[c] Annie Chaussé,[ab] Nathalie Steunou*[c] and Ludovic Legrand*[ab]

Nanocomposites combining the mesoporous iron(III) trimesate MIL-100 (Fe) (MIL: Matériaux Institut Lavoisier) and platinum nanoparticles (Pt-NPs) have been used as immobilization matrices of glucose oxidase (GOx). Due to the physico-chemical properties of Pt-NPs (electroactivity) and MIL-100(Fe) (high specific surface area and pore volume, biocompatibility), the resulting GOx- MIL-100 (Fe)-PtNPs bioelectrode exhibits excellent electrocatalytic performances for glucose detection. This novel glucose biosensor presents a high sensitivity of 71 mA M^{-1} cm^{-2} at optimum condition and a low limit of detection of 5 µM with low response time (< 5 s). In contrast, substitution of iron by chromium or aluminum in MIL-100 leads to a much lower sensitivity and higher response time values, suggesting that the iron centres of MIL-100(Fe) may be involved in a synergic effect which indeed enhances the catalytic oxidation of glucose and biosensor activity. Thus, this work enlarges the potentiality of MOF nanoparticles with engineered cores and surfaces for designing highly sensitive, durable glucose biosensors.

Introduction

Among analytical methods, biosensing of target analytes has received a great attention since the sustainable development of our society requires a strong enhancement of environmental monitoring, food safety, quality control, clinical diagnostics and so on.[1] Electrochemical biosensors which imply the integration of biorecognition elements (*i. e.* enzymes or aptamers) are particularly attractive due to the possibility of performing rapid and one-spot analyses together with a high sensitivity, simplicity and ease of miniaturization.[2,3] However, the use of enzymes in industrial applications is often hampered by their low operational stability, difficult recovery and lack of reusability. One of the key issues for the building-up of biosensors concerns the development of immobilization strategies of biorecognition molecules on solid supports in order to stabilize them in unnatural environment while retaining their functions and activities.[2-4] Therefore, the biocatalytic activity at the surface of the bioelectrodes as well as the mass-transfer efficiency of the relevant analytes are strongly impacted by the interfacial properties between enzymes and the host matrix. Up to now, bioencapsulation in inorganic hosts has concerned mainly metal oxides,[2,4,5,6,7,8] layered double hydroxides or clay minerals[9,10,11] due to their natural origin and/or well-established biocompatibility. Surface adsorption of biomolecules on the host matrix is a simple procedure but leaching of the immobilized enzyme during the reaction process is often observed due to the absence of any specific interactions between the host matrix and enzymes. In contrast, the entrapment of biomolecules in a 3D-matrix strongly reduces this leaching phenomenon but the accessibility to biomolecules and thus the mass-transfer efficiency of analytes may be strongly limited, thereby affecting the sensitivity of biosensors. Therefore, researches on new immobilization matrices is still receiving a great attention and the interest is generally focused on host matrices that combine the following properties: *i)* a hierarchical and well-defined porosity with large pores prone to immobilize enzymes and smaller cavities allowing the diffusion of analytes and products, *ii)* a biocompatibility *iii)* a high surface area favouring a high enzyme loading, *iv)* a chemical and thermal stability under large operating conditions (pH,…), *v)* and if possible, a tuneable composition and surface chemistry that may enhance the anchoring of a large diversity of enzymes at the surface of electrodes.

Metal organic frameworks (MOFs) are crystalline hybrid porous materials formed by the assembly of metal cations with polydentate ligands. In comparison to other inorganic materials, this class of porous materials exhibits a high specific

[a] CNRS UMR 8587 Bd François Mitterrand 91025 Evry, France
[b] Université d'Evry, Laboratoire Analyse et Modélisation pour la Biologie et l'Environnement (LAMBE), Université Evry, Bd François Mitterrand 91025, Evry, France. Email: ludovic.legrand@univ-evry.fr, Tel : +33-1-69-47-7705, Fax : +33-1-69-47-76-55
[c] Institut Lavoisier de Versailles, UMR CNRS 8180, UVSQ, 45 avenue des Etats-Unis 78035 Versailles Cedex. France. Email : nathalie.steunou@uvsq.fr, Tel : +33-1-39-25-43-73, Fax : +33-1-39-25-44-52

† Electronic Supplementary Information (ESI) available: Glucose calibration curves of GOx-MIL-100(Fe)-PtNPs-CIE at different temperatures and pHs, curves of the release of trimesic acid for GOx-MIL-100(Fe)-PtNPs-CIE and MIL-100 (Fe), SEM images of MIL-127(Fe) nanoparticles, glucose calibration curves and chronoamperometric responses of GOx-MOFs-PtNPs-CIE with MOF=MIL-100(Al), MIL-100(Cr) and MIL-127(Fe) See DOI: 10.1039/x0xx00000x

surface and degree of chemical tunability as well as a structural diversity due to the large variety of possible metal cations, organic linkers and building blocks and to the almost infinite number of possible combinations. As a result of their fascinating physico-chemical properties, these materials present potential applications in gas storage/separation,[12,13] catalysis,[14,15,16,17] drug delivery,[18,19] sensors[20,21,22,23] among others. Recently, this class of hybrid materials has emerged as a new type of immobilization matrices for biomacromolecules such as proteins[24,25] and DNA.[26,27,28] Indeed, MOFs appear as promising host matrix candidates due to the possibility of finely tailoring the pore size and functionalizing the pore walls, thereby favouring specific interactions between biomacromolecules and pore walls of MOFs.[29] The incorporation of some micro-enzymes such as MP-11[30] inside the cavities of mesoporous MOFs was first reported and this strategy was enlarged to enzymes (*i. e.* cytochrome C, myoglobin)[31,32] whose molecular dimension exceeds the accessible pore size, revealing the conformational change of protein during transport into the MOFs porosity as a result of the dynamic and flexible structure of protein. The enzyme encapsulation is particularly attractive since it prevents any leaching of enzyme and greatly improves its stability in a wide range of media including non-physiological environments (organic solvents, aqueous solutions of a wide range of pH). However, this method may be limited to a few enzymes and other immobilization strategies have been reported such as adsorption,[33] covalent grafting of proteins at the surface of MOFs particles[34] or host-guest interactions between tag-groups on the enzyme and MOF pores.[35,36] To date a few MOFs-enzymes bioreactors show very promising results in terms of biocatalysis activity, stability and recyclability.[25,32,34,35,37] However, previous works on MOF-based biosensing are comparatively still very scarce.[38,39] While the electrical and electrochemical transduction schemes are commonly used in sensors, they have been minimally explored with MOFs since most of these porous solids are insulating. However, the exploitation of ZIFs (zeolitic imidazolate frameworks) combined to methylene green as a redox mediator for the development of glucose amperometric biosensors has been recently reported in literature and these biosensors present interesting analytical properties in terms of sensitivity (217 mA M^{-1} cm^{-2}) and selectivity.[40] In addition, biosensors based on Cu-MOF and tyrosinase exhibit robust, ultrasensitive and rapid electrochemical responses for the detection of bisphenol A.[41]

Herein, we present the first exploitation of mesoporous metal(III) trimesates (*i. e.* MIL-100 (M) with M=Fe, Al, Cr) and microporous iron(III) azobenzentetracarboxylate MIL-127(Fe) (see Fig. 1) as new and efficient immobilization matrices of enzymes for the building-up of glucose biosensors. The results show that these MOFs can anchor enzymes with high loading/activity and efficient mass-transfer, allowing a highly sensitive detection of glucose. The comparison of the analytical parameters between the different MOFs-based biosensors demonstrate that MIL-100(Fe) is certainly the most efficient host matrix since a synergism of their

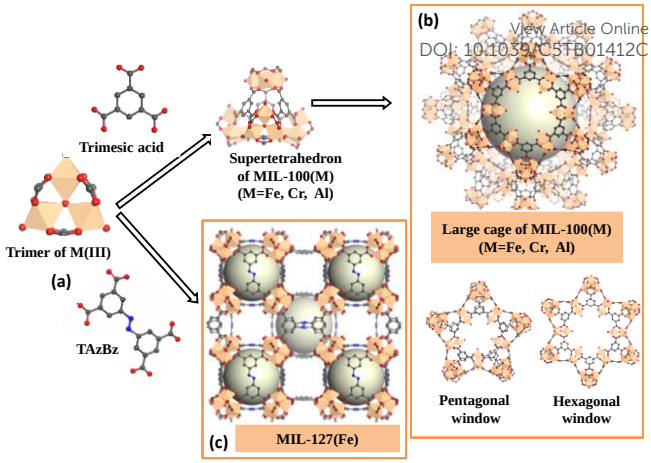

Fig 1. (a) Trimers of Fe(III) octahedra assembled with (b) trimesic acid leading to the formation of the MIL-100 structure with a zeolitic architecture of the MTN-type (c) or with TAzBz (3,3',5,5'-azobenzenetetracarboxylate) leading to a microporous cubic crystalline MIL-127(Fe) structure with a soc topology. The large green spheres represent the largest van der Waals spheres that would fit in the cavities without touching the frameworks.

physico-chemical properties (porosity, electroactivity, morphology, biocompatibility) may enhance both the charge transfer kinetics and the interfacial interactions with enzymes.

Experimental Section

Chemicals and materials

Glucose Oxidase (GOx, EC1.1.3.4, 108 U mg^{-1}, from *Aspergillus niger*), Glutaraldehyde solution (Grade II, 25%), bovine serum albumin (BSA, minimum 98% electrophoresis), D-(β)-glucose, H_2PtCl_6, were purchased from Sigma-Aldrich. Acetate buffer was made from 0.1 M acetic acid and pH was adjusted by adding 4 M NaOH. A stock solution of D-glucose was prepared and allowed to mutarotate at room temperature for 24 h prior to use. All other chemicals and reagents were prepared using millipore water. All reagents were used without further purification.

Pt nanoparticles electrodeposition

For deposition of Pt nanoparticles (PtNPs) on carbon electrode, several experiments were carried out by varying the concentration of H_2PtCl_6, the potential and time of deposition. As a result of these experiments, a solution of 0.002 M H_2PtCl_6 in 0.1 M phosphate buffer (pH=7) and a potential of -0.35 V were chosen for deposition of well-dispersed Pt nanoparticles on carbon electrode, as described in details elsewhere.[42] The electrodeposited mass of Pt was varied from about 2 to 13 µg.cm^{-2} for several experiments.

Synthesis of MIL-100(M) (M=Fe^{3+}, Cr^{3+}, Al^{3+}) and MIL-127(Fe) nanoparticles

The syntheses of mesoporous metal(III) trimesates (metal = Fe^{3+}, Cr^{3+}, Al^{3+}) and MIL-127(Fe) nanoparticles were performed according to previously published procedures.[43,44] Mesoporous metal(III) trimesates were synthesized by microwave-assisted hydrothermal reactions at temperatures between 130 and

210 °C with significant yields within a few minutes only (close to 90 %). Water was used as the solvent which is an advantage in terms of low cost and nontoxicity. For MIL-100(Fe), iron(III) chloride hexahydrate (2.43 g, 8.99 mmol) and trimesic acid (0.84 g, 4.00 mmol) were dissolved in distilled water (30 mL). The solution was heated at 130 °C over 1 min 30 s, then maintained at this temperature for 5 min 30 s (400 W) under high stirring. As soon as the temperature is decreased to 90 °C, 20 mL of water were added to the mixture and the reaction vessel placed in an ice bath to stop the reaction. The mixture was then centrifuged at 10500 rpm for 25 min. An orange solid was thus recovered. The as-synthesized MIL-100(Fe) nanoparticles were washed by four centrifugation/redispersion cycles in absolute ethanol. For MIL-100(Cr), chromium nitrate nonahydrate (2.40 g, 5.99 mmol) and trimesic acid (0.84 g, 4.00 mmol) were dissolved in distilled water (30 mL) with high stirring. The mixture was heated to 200 °C over 4 min and kept at this temperature for 1 min. After cooling, the obtained solid was dispersed in water (20 mL) and then recovered by centrifugation (10500 rpm, 15 min). The solid was activated by dispersing the as-synthesized solid in ethanol for 5 min followed by centrifugation (10500 rpm, 15 min). The redispersion and centrifugation procedures were performed two more times. For MIL-100(Al), aluminum nitrate nonahydrate (1.43 g, 5.68 mmol) and trimesic acid (1.01 g, 4.82 mmol) were dissolved in distilled water (20 mL) with vigorous stirring. After addition of nitric acid (4 mL, 4 M), the reaction mixture was stirred for 5 min at room temperature. After a hydrothermal treatment at 210 °C in the microwave oven for 30 min, the resulting mixture was cooled down with an ice bath and centrifuged at 10500 rpm for 15 min (2.1 g, 98%). MIL-100(Al) was activated by dispersing the recovered solid into methanol overnight with vigorous stirring. The solid was recovered by centrifugation (10500 rpm, 15 min). For MIL-127(Fe), 0.66 mmol of $FeCl_3.6H_2O$ (178.4 mg) and 0.63 mmol of 3,3',5,5'-azobenzenetetracarboxylic acid (H_4-TazBz, 226 mg) were dissolved with moderate stirring in 20 mL of propan-2-ol. This solution was heated in a microwave oven at 130°C (400 W) for 15 min, with a heating ramp of 2 min. The obtained solid was cooled down, then recovered by centrifugation (10500 rpm, 15 min) and washed twice with 40 mL of propanol-2-ol, twice with 40 mL of ethanol and finally, with 20 mL of distilled water. All the synthesized MOFs were characterized by powder X-ray diffraction (PXRD) and FT-IR spectroscopy. The size and surface charge of MOFs nanoparticles were determined by dynamic light scattering (DLS) and ζ-potential measurements. The composition and purity of MOFs nanoparticles were confirmed by thermogravimetric analyses (TGA) and FT-IR. Their specific surface was estimated by nitrogen porosimetry at 77 K.

Instrumentation and physical-electrochemical characterizations

The potentiostat used was an EG & G PAR VersaSTAT 3 controlled with a computer using the software VersaStudio package. Carbon ink electrodes (CIE) were prepared by painting carbon ink (made by Acheson) with a brush on 20 mm diameter stainless steel disk. The surface area in contact with electrolyte is 3 cm^2. The AgCl/Ag reference electrode was home-made by electrolysis of Ag wire in 5 M NaCl for 5 min at 5 mA cm^{-2}. The counter electrode was a Nickel mesh. The pH of the solution was measured at room temperature with a pH-meter (model: WTW – pH340i). For chronoamperometric experiments, a Metrohm 802 Stirrer rotator was rotating to increase mass transport while measuring the currents with respect to duration of the experiments. Various volumes of 0.05 M glucose from 1 µL to 100 µL were added drop wise in the solution of electrolyte (*i. e.* acetate buffer of pH≈5.3). The temperature of the electrochemical cell was controlled at 37°C by a POLYSTAT 5hp thermostat (Bioblock Scientific). FT-IR spectra were recorded using a Bruker IFS28 FTIR spectrometer equipped with a reflection absorption tool (Grazeby Specac) that allowed us to analyze the film directly on the disc surface without scraping procedure. The background measurement was taken with a gold disc that had been mirror-like polished. Twenty scans were performed for background and samples. Dynamic light scattering (DLS) measurements were performed on a Malvern Zetasizer Nano-ZS ZEN 3600. Scanning electron microscopy (SEM) images have been recorded on a JEOL JSM-7001F microscope using gold-coated samples. Powder X-ray diffraction patterns (PXRD) were collected using a Siemens D5000 diffractometer (θ–2θ) with Cu K_α radiation (λ = 1.54059 Å). Surface area of the materials was determined by N_2 adsorption using BJH method in a BELSORP-mini II porosimeter at 77 K using nitrogen as a probing gas.

Preparation of bioelectrodes

The preparations of bioelectrodes were performed by a step-by-step deposition of various components at the surface of CIE. First, CIE was decorated by PtNPs particles by electrodeposition as described above. Then, solutions of MOFs and GOx were successively deposited at the surface of PtNPs-CIE to permit the formation of layers of MOF and GOx. Prior to the MIL-100(Fe) deposition at PtNPs-CIE, solutions of MIL-100(Fe) nanoparticles (2 mg mL^{-1}) at pH 3.5 were sonicated for 5 min. The resulting suspension was allowed to settle for 30 min in order to separate the aggregates at the bottom of the container. Then, 100 µL of the supernatant (0.7 mg. mL^{-1} of MOF) was drop casted on the PtNPs-CIE followed by drying at 50°C oven for one hour. In a second step, 100 µL of 12 mg mL^{-1} GOx dissolved in acetate buffer (pH=5.3) was then deposited on MIL-100(Fe)-PtNPs-CIE and dried at 50°C for 1 hour. No difference of sensitivity was evidenced between bioelectrodes dried at room temperature and those dried at 50°C (see Fig. SI1 of ESI). Finally, the electrodes were coated with a protective layer made of glutaraldehyde as a crosslinker and bovine serum albumin by dropping 50 µL of mixture of glutaraldehyde (25 mg mL^{-1}) and bovine serum albumin (40 mg mL^{-1}) solutions with a volume ratio of 1:3 onto the surface of MIL-100(Fe)-PtNPs-CIE. Following the same procedure, other bioelectrodes were prepared either without MOF (i. e. GOx-PtNPs-CIE) or with other MOFs nanoparticles (i. e. MIL-100(Al)-

View Article Online
DOI: 10.1039/C5TB01412C

GOx-PtNPs-CIE, MIL-100(Cr)-GOx-PtNPs-CIE, MIL-127(Fe)-GOx-PtNPs-CIE).

Stability of MOF electrodes

The stability of MIL-100(Fe) nanoparticles at the surface of PtNPs-CIE in acetate buffer (pH=5.3) was studied according to a protocol previously reported in literature.[45] A known amount (1.3 mg) of MIL-100(Fe) powder was suspended in 10 mL of acetate buffer for durations between 2 hours and 6 days. For monitoring the initial period of degradation, an aliquot of 1 mL of supernatant was recovered and replaced with the same volume of fresh acetate buffer every 2 hours up to 8 hours, and thereafter every 24 hours. Equivalent experiments were performed also on MIL-100(Fe)-CIE electrodes, at the surface of which a defined amount of MIL-100(Fe) is deposited. These electrodes were kept at 0.5 V for 3 days in acetate buffer and similarly aliquots were withdrawn at regular interval of times for measuring the released trimesic acid. Released trimesic acid was quantified in the supernatant by high performance liquid chromatography (HPLC). Experiment was done in triplicate. The concentration of the delivered trimesic acid was determined using a RP-HPLC system (Reversed phase liquid chromatography) Alliance Waters equipped with a PDA spectrophotometer detector at λ= 215 nm.

Results and discussion

Description of MOFs

Nanoparticles of MIL-100(Fe) have been prepared by a microwave assisted 'non-HF' hydrothermal synthesis, as previously described[43] and further characterized. MIL-100(Fe) is an iron(III) carboxylate with a highly porous 3D structure formed by the assembly of oxo-centered trimers of iron octahedra and trimesate ligands. The association of these two moities leads to hybrid supertetrahedral (ST) units that further assemble into a zeolitic architecture of MTN-type. This topology contains interconnected mesoporous cages of free apertures of ca. 25 and 29 Å accessible through microporous windows (5.6 Å and 8.6 Å) (Fig. 1). Moreover, due to the presence of accessible unsaturated Lewis acid iron sites that may be coordinated by different species, MIL-100(Fe) may be interesting for different applications such as catalysis, separation, and biomedicine.[15,18,19,46] The N_2 adsorption measurements at 77 K of MIL-100(Fe) nanoparticles indicate a high BET specific surface area of 1350 m^2 g^{-1}. MIL-100(Fe) nanoparticles exhibit a well-faceted octahedral morphology and a mean diameter of 130 ± 30 nm as determined by combining TEM (Fig. 2) and DLS at pH = 5.3 (see Table 1). Since the isoelectric point (IEP) of GOx lies between 3.9 and 4.3 and the point of zero charge of MIL-100(Fe) is close to 4, no attractive electrostatic interactions may be expected at pH=5.3 between MIL-100(Fe) nanoparticles and GOx.

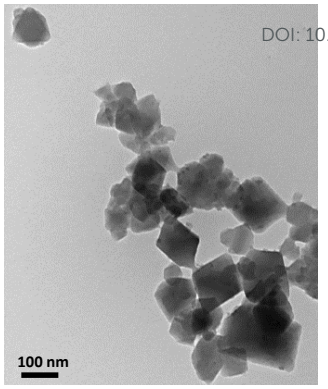

Fig. 2. TEM image of MIL-100(Fe) nanoparticles.

Characterization of GOx-MIL-100(Fe)-PtNPs-CIE

Pt or glassy carbon electrodes are commonly used in most of the glucose biosensors reported so far in literature. However, in the present work, a small amount of platinum nanoparticles (PtNPs) have been deposited at the surface of carbon ink electrode (CIE), thereby decreasing the cost of the biosensor. Moreover, it is known that using PtNPs for glucose oxidation leads to tremendous improvement in glucose detection.[47] To assess the preservation of the secondary structure of GOx immobilized on MIL-100(Fe), FTIR spectra were recorded since the amide I (1700-1600 cm^{-1}) and II (1600- 1500 cm^{-1}) IR bands of GOx are generally used for monitoring conformational changes of proteins.[48,49] The IR vibration band of amide I is due to stretching vibration of C=O of peptide linkages in the protein backbone while that of amide II is the combination effect of bending of N-H and stretching of C-N of peptide groups.[48,49] The FTIR spectra of GOx-MIL-100(Fe)-CIE (Fig. 3, curve iv) exhibits both characteristic bands at 1672 (amide I), 1561 cm^{-1} (amide II which is partially overlapped by the IR band ν(C=O) of trimesate ligand) and 1090 cm^{-1} (C-O bond stretching vibration of GOx) in addition to the bands present in the spectrum of MIL-100(Fe)-CIE (curve ii). It is worth noting that the band positions are slightly shifted compared to those of GOx-CIE (Fig. 3, curve iii) but are in agreement with the already reported values in literature.[50]

Table 1. Structural properties of MOFs nanoparticles used as host matrices for GOx .

MOFs	d_{pore} (Å)	d_{window}(Å)	S_{BET}($m^2.g^{-1}$)	$d_{particle}$(nm)[a]	ζ-pot (mV)[b]
MIL-100(Fe)	25-29	5.6-8.6	1350	130	-10
MIL-100(Cr)	25-29	5.6-8.6	1400	10	-27
MIL-100(Al)	25-29	5.6-8.6	1700	100	-20
MIL-127(Fe)	6-10	4	1390	400	-19

[a]determined by TEM;[43 b] ζ-potential measured at pH=5.1

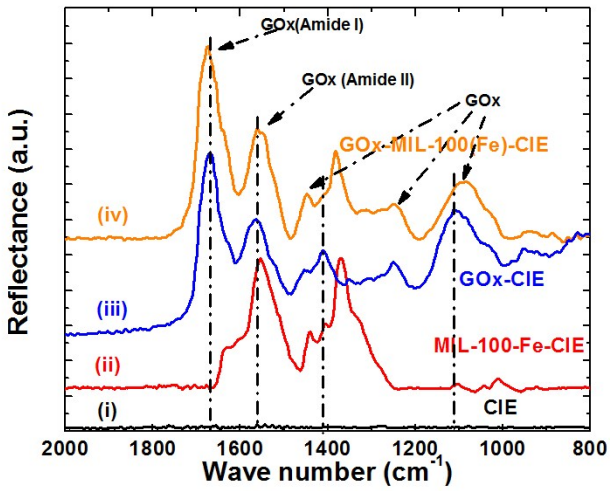

Fig. 3 FT-IR spectra of (i) CIE, (ii) MIL-100(Fe)-CIE, (iii) GOx-CIE and (iv) GOx-MIL-100(Fe)-CIE (all spectra are baseline-corrected).

This observation suggests that GOx is not denatured after immobilization in the MOF matrix.

Fig. 4 shows a series of SEM images of modified electrodes obtained by the successive deposition of each layer (PtNPs, MOFs and GOx). Fig. 4(a) shows a typical image of CIE with a rough surface. As shown in Fig. 4(b), the electrochemically deposited Pt nanoparticles (PtNPs) with an average size close to 130 nm are particularly well-dispersed on CIE. By drop-casting the colloidal solution of MIL-100(Fe) on the PtNPs-CIE, the surface of the modified electrode is uniformly covered by a few MIL-100(Fe) aggregates (Fig. 4(c)). This morphology is not affected after GOx immobilization (Fig. 4(d)).

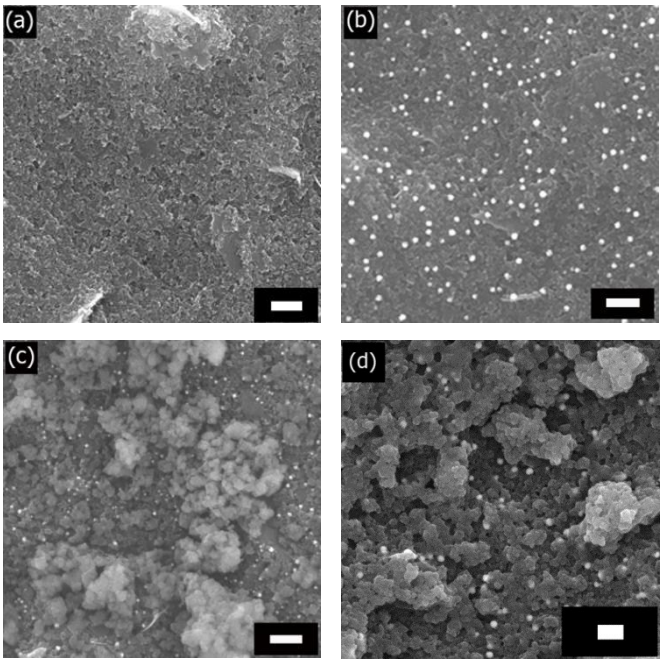

Fig. 4. SEM images of modified electrodes, (a) CIE, (b) PtNPs-CIE, (c) MIL-100(Fe)-PtNPs-CIE and (d) GOx-MIL-100(Fe)-PtNPs-CIE. The scale bar represents 1 μm.

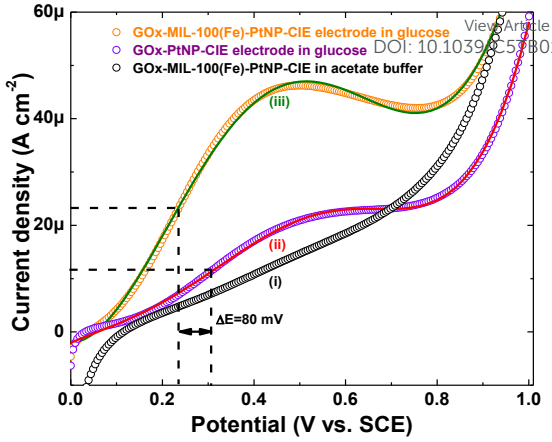

Fig. 5. Linear sweep voltammograms of the electrodes in air-saturated 0.1 M acetate buffer (pH=5.3) (i) GOx-MIL-100(Fe)-PtNp-CIE (ii) GOx-PtNp-CIE after addition of 0.5 mM glucose and (iii) GOx-MIL-100(Fe)-PtNp-CIE after addition of 0.5 mM glucose. Symbols represented are the experimental points and the solid lines correspond to fits of data.

Preliminary voltammetry study

First, the electrochemical detection of glucose at GOx-MIL-100(Fe)-PtNPs-CIE was compared with a modified electrode without MIL-100(Fe). Fig. 5 shows linear sweep voltammograms of GOx-PtNPs-CIE and GOx-MIL-100(Fe)-PtNPs-CIE in 0.5 mM glucose/0.1 M acetate buffer solution. In presence of glucose, the cyclic voltammogram of GOx-PtNPs-CIE shows a peak at 0.55 V due to oxidation of H_2O_2 (product of glucose oxidation,) whose peak current density is close to 23 μA cm^{-2} (curve ii). Noteworthy, one can point out that (i) a two-fold increase of peak current density (~46 μA cm^{-2}) and (ii) a slight shift of the half wave potential are observed when the electrode contains MIL-100(Fe) as host matrix (Fig. 5 curve iii). This is a clear indication that the presence of MIL-100(Fe) improves the electro-oxidation of H_2O_2. The cyclic voltammetry experiments suggest that MIL-100(Fe) impacts significantly the performance of glucose biosensor possibly due to the high amount of electrochemically accessible GOx as a result of the high surface area and porosity of MIL-100(Fe). Additionally, the influence of MIL-100(Fe) on the detection of glucose may be strongly related to the role of Fe(III) centres in the catalytic process (see *vide infra*).

Glucose biosensing performance of GOx-MIL-100(Fe)-PtNPs-CIE

The glucose sensing performance of the GOx-MIL-100(Fe)-PtNPs-CIE was estimated by typical chronoamperometric (CA) measurements in air-saturated stirred acetate buffer at pH=5.3 and a fixed potential of 0.5 V (this potential value has been chosen as it corresponds to the maximum current density of the cyclic voltammogram, see Fig. 5). An increase of the current density is observed for GOx-MIL-100(Fe)-PtNPs-CIE after each addition of an aliquot of 0.05 M glucose solution, with a time interval of 200 s (Fig. 6(a)). The current response increases linearly with increasing the glucose concentration from 5 μM to 1.4 mM, with a high sensitivity of 71 mA M^{-1} cm^{-2} (Fig. 6(b)) and a correlation coefficient of 0.996. The GOx-MIL-100(Fe)-PtNps-CIE can achieve 90% of the steady-state current

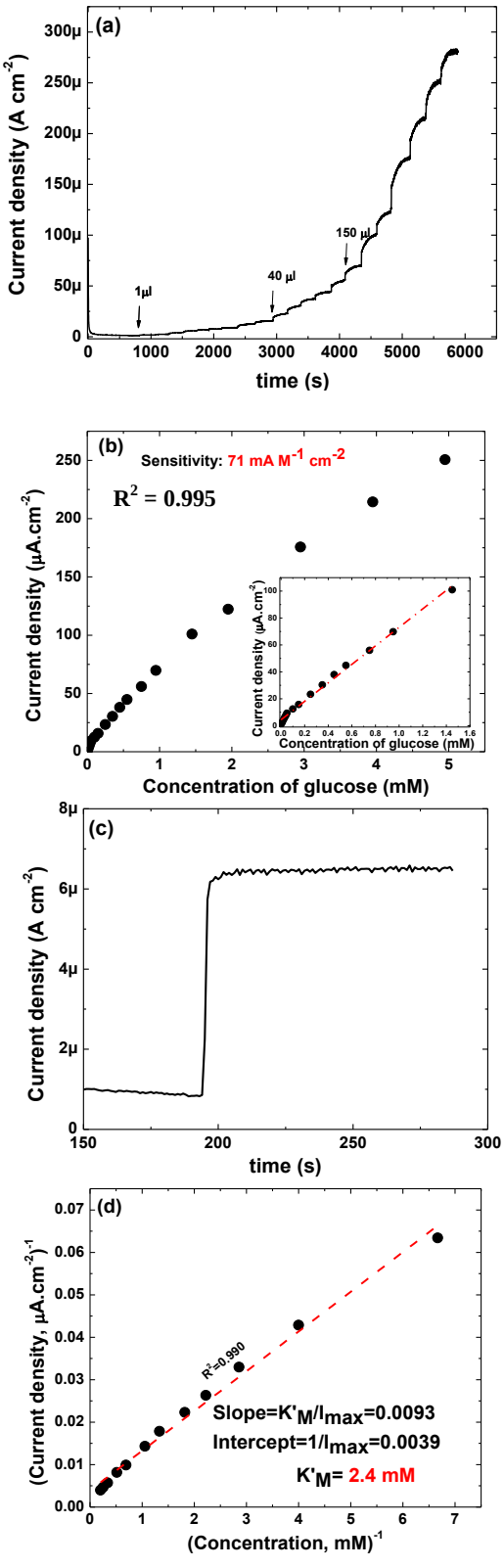

Fig. 6. (a) Current density-time curve of a GOx-MIL-100(Fe)-PtNPs -CIE for successive addition of 0.05 M of glucose aliquots to vigorously stirred 0.1 M air-saturated acetate buffer (pH = 5.3) at the potential of 0.5 V. (b) Glucose calibration curve of current vs glucose concentration from the curve a) and fit of data in the inset, (c) response time determination by adding 0.08 mM glucose and (d) the Lineweaver-Burk plot obtained from the amperometric response in (a).

only within <5 s, indicating a fast response for glucose sensing (the response time of the electrode was measured by adding a glucose concentration of 0.08 mM to a fresh electrode) as depicted in Fig. 6(c). In order to evaluate the biological activity of immobilized GOx enzyme on biosensor surfaces, the effective or apparent Michaelis–Menten constant (K'_m) is often determined amperometrically from the Lineweaver–Burk-type equation,

$$\frac{1}{I_{SS}} = \frac{K'_m}{I_{max}} \times \frac{I}{C} + \frac{1}{I_{max}} \quad (1)$$

Equation (1) represents a rearrangement of Equation 24b from Shu and Wilson,[51] where I_{max} and I_{ss} are the currents measured for enzymatic product detection under conditions of substrate saturation and steady state, respectively, for a given substrate concentration, C. A plot of $1/I_{SS}$ vs $1/c$ will give a straight line with the slope equal to K'_m/I_{max} and intercept equal to $1/I_{max}$. K'_m is determined to be 2.4 mM from the intercept and slope of the Lineweaver-Burk plot (Fig. 6(d)), a value that is lower than the K'_m values reported for free GOx of 33-110 mM.[52] A low K'_m value usually suggests that the enzyme may have a high affinity with the substrate. A high sensitivity together with a low limit of detection and a low apparent Michaelis–Menten constant suggests that the GOx/MIL-100(Fe)/PtNPs-modified carbon biosensor creates an exceptional biocompatibility micro-environment for enzymatic biosensing.[51]

Optimization and stability of GOx-MIL-100(Fe)-PtNPs-CIE biosensors

The various parameters which affect the sensitivity of biosensor are gathered together in Fig. 7. The parameters such as pH of the solutions (Fig. 7(a)), amount of PtNPs (Fig. 7(b)) and GOx (Fig. 7(c)) on the electrode surface were studied. The pH of the solution in which the sensitivity of the biosensor was measured has tremendous effect on the activity of biosensor.[53] Three pH values (4, 5.5 and 7) were studied (Fig. 7(a)). The highest activity of 71 mA M^{-1} cm^{-2} was observed in acetate buffer at pH 5.3, a value close to the pH of optimum activity (i.e. pH 5.5) of native GOx supplied from Sigma-Aldrich. Moreover, the pH of the solution in which GOx was solubilized to drop cast on the electrode was varied between 3.5 and 7 (see Fig SI2 of ESI). The highest sensitivity is also observed for an initial GOx solution of pH 5.3. Although in the literature most of the glucose titration was performed at pH 7, our study reveals that the biosensor activity is considerably low at this particular pH (0.1 M HEPES buffer). It is noteworthy that a phosphate buffer could not be used in the presence of MIL-100(Fe) due to the rather fast degradation of this MOF in this buffer as reported previously throughout biomedical studies.[45] Therefore, to assess the stability of MIL-100(Fe), the MIL-100(Fe)-CIE electrode was left in 0.1 M acetate buffer (pH=5.3) for 3 days at 0.5 V. These storage conditions are similar to those commonly used for glucose sensing. The amount of trimesic acid linker released in acetate buffer was determined

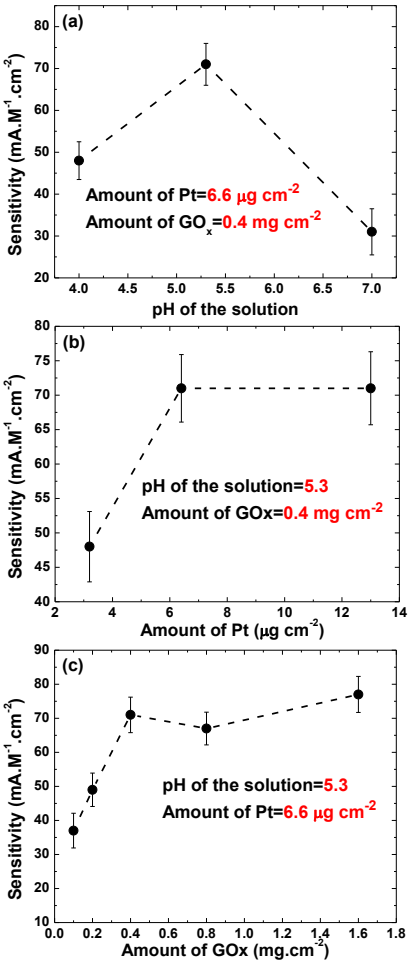

Fig. 7. Variation of sensitivity for glucose sensor with (a) pH of the measuring solution, (b) amount of Pt and (c) amount of the enzyme GOx. Data points are connected by a dashed line which should be used as a guide for the eyes.

by HPLC and the quantification of MIL-100(Fe) nanoparticles which are dissociated in acetate buffer evaluated. In comparison to MIL-100(Fe) nanoparticles directly dispersed in acetate buffer and for which 30% of nanoparticles are dissociated, the degradation ratio reaches only about 2% for MIL-100(Fe) nanoparticles immobilized at the surface of PtNPs-CIE (see Fig. SI3 of ESI). It was also observed that the amount of PtNPs has a significant impact on the sensitivity of our biosensor (Fig. 7(b)). From 0 to 5.5 µg cm^{-2} of Pt, an increase of the electrode sensitivity is observed. Beyond, a plateau is reached, indicating that a Pt amount of 5.5 µg cm^{-2} corresponds to the minimal number of oxidation centres required to match the flow of H_2O_2. The impact of the amount of GOx is also represented in Fig. 7(c). By increasing the GOx amount, the sensitivity of the glucose biosensor increases to a maximum corresponding to an optimal GOx amount of 0.4 mg cm^{-2} for which electrochemically accessible enzymes have reached saturation. To evaluate the stability of the biosensor, current density of the GOx-MIL-100(Fe)-PtNPs-CIE was monitored over a period of 3 weeks (Fig. 8). The current

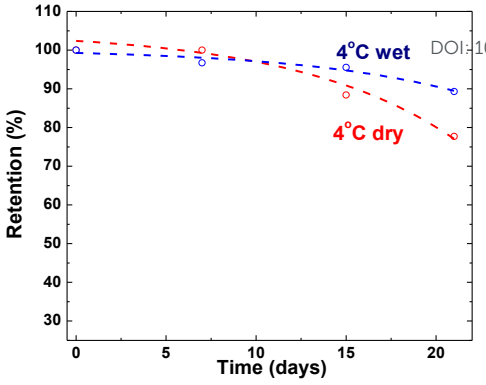

Fig. 8. Storage stability of the GOx-MIL-100(Fe)-PtNPs-CIE at pH=5.3 which is compared with the electrode kept in dry conditions at 4°C.

density was measured at an interval of 7 days in 0.25 mM glucose of acetate buffer solution at pH=5.3. The electrodes were washed with acetate buffer solution and stored after use at 4 ºC under dry and wet conditions. The GOx-MIL-100(Fe)-PtNPs-CIE was able to retain more than 96% of its original current response over a storage period of 1 week, and up to 90% and 78% when aged for 21 days in wet and dry conditions, respectively. Five electrodes, made independently following the same procedure, showed a reproducibility of 5 %, confirming the robustness of our preparation method.

The selectivity of the GOx-MIL-100(Fe)-PtNPs-CIE biosensor was finally investigated. As documented in previous works on glucose biosensor,[9,11,47] a variety of electroactive species such as ascorbic acid (AA), uric acid (UA) and dopamine (DA) may potentially interfere with the detection of glucose. As shown in Fig. SI.4, the addition of 0.1 mM AA and UA leads to a negligible current increase. In contrast, the interference exerted by DA on the glucose detection is much stronger. In the present study, the glucose detection is based on the electrooxidation of enzymatically generated H_2O_2 which requires a quite high polarizing voltage applied (E_{app} = 0.5 V). As reported previously, this interference phenomenon on glucose detection may be notably reduced through the immobilization of a redox mediator (i. e. ferrocene anion, methyl viologen…).[9,11]

Comparison of glucose biosensing properties

The performance of GOx-MIL-100(Fe)-PtNPs-CIE seems superior to bioelectrodes based on ZIF-8 and glucose dehydrogenase in terms of the sensitivity and linear range parameters according to the analytical parameters previously reported *(i. e.* linear range of 0.1-2 mM, sensitivity of 54 mA M^{-1} cm^{-2}).[40] The LOD value is similar to those of numerous glucose biosensors but higher than that of reported for glucose sensors based on pure Fe(III)-MOFs.[65] The biosensor performance can also be compared to those reported for other glucose biosensors based on metal oxide/Pt electrodes (Table 2). The sensitivity of the present biosensor is higher than other GOx biosensors based on metal oxides (ZrO_2, TiO_2, SiO_2) (see Table 2). Due to the possible presence of fractures in sol-gel metal oxide based films upon drying, composite

View Article Online
DOI: 10.1039/C5TB01413C

biofilms were previously reported by casting mixtures of organic polymers (chitosan or Nafion) and metal oxides.[54,55] As indicated in Table 2, the addition of nafion to the bioelectrodes strongly enhances the sensitivity of the biosensor response. However, except for TiO_2-Nafion electrode, the sensitivity of SiO_2/ZrO_2-Nafion based biosensors is comparable or even lower than MIL-100(Fe)-PtNPs-CIE. In order to possibly unravel the origin of the biosensing performance of GOx-MIL-100(Fe)-PtNPs-CIE (high sensitivity, low response time and large linear range of concentration), similar bioelectrodes have been prepared with other MOFs following the same procedure and the analytical parameters of biosensors were compared (see Table 3). Other mesoporous metal(III) trimesates and a microporous Fe(III) MOFs (i. e. MIL-127(Fe)), exhibiting the same building unit as MIL-100, were used as immobilization matrices of GOx. Table 1 presents the structural properties of these MOFs. MIL-100 (Al) and MIL-100 (Cr) exhibit also the crystalline mesoporous MIL-100 type structure but in contrast to MIL-100(Fe), these phases are built-up by the connectivity of trimers of electrochemically inert trivalent cations (Al^{3+} and Cr^{3+}). As reported previously, the BET specific surface area of pure water-synthesized MIL-100(Al) and MIL-100(Cr) is quite high (typically 1700 and 1400 m^2 g^{-1} respectively). Similarly to its isostructural iron analog, MIL-100(Al) nanoparticles exhibit a well-faceted octahedral shape with an average diameter of 100 nm close to that of MIL-100(Fe) nanoparticles (130 nm).[43] In contrast, the MIL-100(Cr) nanoparticles are definitely smaller (diameter of 10 nm), as revealed by the TEM observations and the gel-like properties of the sample as previously reported.[43] It is noteworthy that for the three MIL-100 analogs, diameters of nanoparticles determined by DLS are larger than that observed by TEM as a result of a possible aggregation phenomenon in aqueous solution which is particularly remarkable for the MIL-100(Cr) nanoparticles. According to the negative surface charge of MIL-100(Cr) and MIL-100(Al) nanoparticles (see the ζ-potential values in Table 1) in aqueous solution at pH=5.3, no attractive electrostatic interactions may be expected with GOx (IEP~3.9). As shown in Fig. 1, the inorganic building units of MIL-127(Fe) are oxo-centered trimers of Fe(III) octahedra similar to those of MIL-100(Fe). However, the assembly of these trimers with the 3,3',5,5'-azobenzenetetracarboxylate ligand (TazBz) leads to a microporous cubic crystalline structure with a *soc* topology. This structure contains two types of cavities, namely an accessible 1D channel system (~ 5-7 Å) and cages of *ca.* 10 Å, accessible through open apertures of ~3 Å. The MIL-127(Fe) nanoparticles exhibit a cubic morphology with a mean diameter of 400 nm which is about three fold higher than that of MIL-100(Fe) nanoparticles. In contrast to MIL-100 analogs, the nanoparticles of MIL-127(Fe) are more polydisperse in size since a few smaller nanoparticles can be also observed by SEM (~150 nm) (see Fig SI5 of ESI). In contrast to GOx-MIL-100(Fe)-PtNPs-CIE, the glucose calibration curves of GOx-MOFs-PtNPs-CIE (MOFs= MIL-100 (Cr), MIL-100(Al) and MIL-127(Fe)) (see Fig. SI6 of ESI) present a non-linear part for a small glucose concentration (< 100 μM), a linear response in the range 100-1000 μM followed by a saturation regime. This electrochemical response and the high response time (> 50 s) (see Fig. S17 of ESI) are consistent with a slower diffusion of H_2O_2 at the surface of these bioelectrodes in comparison to GOx-MIL-100(Fe)-PtNPs-CIE. Therefore, by comparing the analytical parameters of GOx-MOFs-PtNPs-CIE (see Table 3), the biosensor prepared with MIL-100(Fe) appears superior in terms of sensitivity, detection time, linear concentration range and limit of detection.

As a consequence, it seems that MIL-100(Fe) nanoparticles combine the physico-chemical properties that allow a fast and sensitive detection of glucose. First, by comparing the results of MIL-100(Fe) and MIL-127(Fe) which are both MOFs based on oxo-centered iron centers, it may be suggested that the presence of MIL-100(Fe) may enhance the kinetics of charge transfer due to the smaller size of nanoparticles (100 vs 400 nm) and the larger pore diameter (24-29 Å vs 6-10 Å). However, the high electrochemical performance of MIL-100(Fe) cannot be only explained by its mesoporous trimesate

Table 2. Analytical parameters of GOx-MIL-100(Fe)-PtNPs-CIE along with other glucose based biosensors.

Electrode material	Sensitivity ($mA\ M^{-1}\ cm^{-2}$)	Response time (s)	Ref [a]
Pt-Fe_3O_4-Cs[b]-Nf[c]	11.5	Not reported	56
GOx/Cs[b]-Fe_3O_4/FTO[d]	1.2	Not reported	57
ZrO_2	1.42	<5	54
SiO_2	17.6	Not reported	55
$K_2[V_6O_{16}]$	48	15	58
V_2O_5	17	15	58
ZrO_2/Cs[a]	0.89	<10	59
TiO_2/ Cs[a]	9.25	10	60
ZrO_2/ Nf[c]	48	Not reported	54
TiO_2- Nf[c]	105.7	Not reported	55
SiO_2- Nf[c]	71.7	Not reported	55
ZnO/Pt/Cs[b]/GOx	62.14	Not reported	61
GOx-Mg-Fe-CO_3[e]-Pt	39	15	62
MIL-100(Fe)-PtNPs	71	<5	Ow[f]

[a] references; [b] Cs : Chitosan; [c] Nf : Nafion; [d] FTO: fluorine doped tin oxide; Mg-Fe-CO_3: Layered double hydroxide (LDH); [f] our work

Table 3. Comparison of electroanalytical properties of GOx-MOF-PtNPs-CIE

Modified electrode	MOF	S[a] ($mA.\ M^{-1}.cm^{-2}$)	RT[b] (s)	LCR[c] (μM)	LOD[d] (μM)
GOx-MOF-PtNPs-CIE	MIL-100(Fe)	71	<5	5 -1400	5
	MIL-100(Cr)	37	>50	100- 1000	10
	MIL-100(Al)	22	>50	100-1000	20
	MIL-127(Fe)	29	>50	100 -1000	20

[a] sensitivity; [b] response time; [c] linear concentration range; [d] limit of detection was calculated by taking Signal (S) to Noise (N) ratio as 3.

MIL-100 type framework according to the poor results obtained with the Al and Cr analogs. These results suggest that electroactive or catalytic species in the host matrix are also required for a fast and sensitive electrochemical response. Actually, it has been recently reported that iron(III) based MOFs such as MIL-100(Fe), MIL-68(Fe), MIL-53(Fe) and MIL-88B-NH_2(Fe) exhibit intrinsic peroxidase-like activity and are thus able to catalyse oxidation of compounds in the presence of H_2O_2.[63,64,65] Since H_2O_2 is the main product of glucose oxidation by GOx, the superior performance of MIL-100(Fe) based bioelectrodes may be explained by a synergy of catalytic activity between GOx and MIL-100(Fe), as previously reported for the colorimetric detection of glucose by combining GOx and MIL-88B-NH_2(Fe).[65] It was previously reported that iron(III) based MOFs may induce $^{\cdot}OH$ radical formation by catalyzing the decomposition of H_2O_2 by a Fenton-type reaction.

Conclusions

In the present work, we have shown that bioelectrodes based on biocompatible MOFs such as MIL-100(Fe) and GOx supported on platinium nanoparticules (PtNP) can be used as glucose amperometric biosensors with very interesting properties in terms of sensitivity (71 mA M^{-1} cm^{-2}), response time (<5 s), reproducibility, stability in time and operating/storage conditions. Various physico-chemical parameters such as pH of the measuring solution, amount of PtNP and GOx were varied to obtain optimized bioanalytical responses. By comparing the glucose biosensing properties of mesoporous metal (III) trimesates (with metal=Fe, Cr, Al) and MIL-127(Fe), it appears that MIL-100(Fe) based biosensor exhibits superior performance as result of a synergism of physico-chemical and microstructural properties of MIL-100(Fe) (mesoporosity, biocompatibility, size of nanoparticles…) and catalytic properties of Fe^{3+} centres and GOx. In particular, Fe^{3+} cations of MIL-100(Fe) may exhibit intrinsic peroxidase-like activity. These results show that Fe based MOFs may presumably compete with other inorganic host matrices for enzyme immobilization through the optimization of the biosensor preparation. Given the variety of proteins and the range of possible biocompatible MOFs candidates, this method for the preparation of protein-MOF bioelectrodes opens numerous perspectives for combining together their properties and functionalities and designing novel nanodevices such as biosensors or biofuel cells operating in a large range of conditions, even at low pH values.

Acknowledgements

Author acknowledges the contribution of Dr. Carine Livage for performing the scanning electron microscopy of the electrodes. Authors also thank the (ANR-11-LABEX-0039) for funding the postdoctoral fellowship. N.S. would like to thank Dr Christine Mousty (ICCF, Clermont-Ferrand) for fruitful discussions regarding glucose biosensing.

Notes and references

View Article Online
DOI: 10.1039/C5TB01412C

1 (a) G. Konvalina, H. Haick, *Acc. Chem. Res.*, 2014, **47**, 66-76; (b) N. Shehada, G. Brönstrup, K. Funka, S. Christiansen, M. Leja, H. Haick, *Nano Lett.,* 2015, **15**, 1288−1295; (c) B. Wang, J. C. Cancilla, J. S. Torrecilla, H. Haick, *Nano Lett.,* 2014, **14**, 933−938.

2 (a) M. Hartmann and X. Kostrov*, Chem. Soc. Rev.*, 2013, **42**, 6277-6289; (b) M. Hartmann and D. Junk, *J. Mater. Chem.*, 2010, **20**, 844-857; (c) D. Avnir, S. Braun, O. Lev and M. Ottolenghi, *Chem. Mater.*, 1994, **6**, 1605-1614.

3 (a) M. Darder, P. Aranda, E. Ruiz-Hitzky, *Adv. Mater.*, 2007, **19**, 1309-1319; (b) M. Darder, P. Aranda, M. L. Ferrer, M. C. Gutiérrez, F. del Monte, E. Ruiz-Hitzky, *Adv. Mater.*, 2011, **23**, 5262-5267; (c) B. Wicklein, M. Darder, P. Aranda, E. Ruiz-Hitzky, *ACS Appl. Mater. Interfaces,* 2011, **3**, 4339-4348.

4 D. Avnir, T. Coradin, O. Lev and J. Livage, *J. Mater. Chem.*, 2006, **16**, 1013-1030.

5 A. C. Pierre, *Biocatal.Biotransfor.*, 2004, **22**, 145-170.

6 (a) M. I. Shukoor, F. Natalio, H. A. Therese, M. N. Tahir, V. Ksenofontov, M. Panthöfer, M. Eberhardt, P. Theato, H. C. Schröder, W. E. G. Müller and W. Tremel, *Chem. Mater.* 2008**,** **20***,* 3567–3573 ; (b) R. André, M. N. Tahir, H. C. C. Schröder, W. E.G. Müller and W. Tremel, *Chem. Mater.,* 2011, **23**, 5358−5365.

7 (a) V. V. Vinogradov and D. Avnir, *RSC Adv.*, 2015, **5**, 10862–10868; (b) V. V. Vinogradov and D. Avnir, *J. Mater. Chem. B*, 2014, **2**, 2868-2873.

8 (a) A. Walcarius, *Electroanal.*, 2015, **27**, 1303-1340; (b) I. Mazurenko, W. Ghach, G. W. Kohring, C. Despas, A. Walcarius, E. Mathieu, *Bioelectrochem.*, 2015, **104**, 65-70.

9 C. Mousty, *Appl. Clay Sci.*, 2004, **27**, 159-177.

10 C. Forano, S. Vial and C. Mousty, *Curr. Nanosci.*, 2006, **2**, 283-294.

11 C. Mousty, *Anal. Bioanal. Chem.*, 2010, **396**, 315-325.

12 L. J. Murray, M. Dinca and J. R. Long, *Chem. Soc. Rev.*, 2009, **38**, 1294-1314.

13 (a) P. L. Llewellyn, M. Garcia-Rates, L. Gaberova, S. R. Miller, T. Devic, J.-C. Lavalley, S. Bourrelly, E. Bloch, Y. Filinchuk, P. A Wright, C. Serre, A. Vimont, G. Maurin, *J. Phys. Chem. C*, 2015, **119**, 4208-4216; (b) Q. Y. Yang, S. Vaesen, F. Ragon, A. D. Wiersum, D. Wu, A. Lago, T. Devic, C. Martineau, F. Taulelle, P. L. Llewellyn, H. Jobic, C. L. Zhong, C. Serre, G. De Weireld and G. Maurin, *Angew. Chem. Int. Edit.,* 2013, **52**, 10316-10320.

14 J. Y. Lee, O. K. Farha, J. Roberts, K. A. Scheidt, S. B. T. Nguyen and J. T. Hupp, *Chem. Soc. Rev.*, 2009, **38**, 1450-1459.

15 P. Horcajada, S. Surblé, C. Serre, D.-Y. Hong, Y.-K. Seo, J.-S. Chang, J.-M. Grenèche, I. Margiolaki and G. Férey, *Chem. Commun.*, 2007, **27,** 2820-2822.

16 (a) J. Gascon, U. Aktay, M. D. Hernandez-Alonso, G. P. M. van Klink, F. Kapteijn, *J. Catal.*, 2009, **261**, 75–87; (b) M. A. Nasalevich, R. Becker, E. V. Ramos-Fernandez, S. Castellanos, S. L. Veber, M. V. Fedin, F. Kapteijn, J. N. H. Reek, J. I. van der Vlugt, J. Gascon, *Energy. Environ. Sci.*, 2015, **8**, 364-375.

17 C. Rösler, R.A. Fischer , *Cryst.Eng.Comm.* **2015**, *2*, 199-217.

18 P. Horcajada, T. Chalati, C. Serre, B. Gillet, C. Sebrie, T. Baati, J. F. Eubank, D. Heurtaux, P. Clayette, C. Kreuz, J.-S. Chang, Y. K. Hwang, V. Marsaud, P.-N. Bories, L. Cynober, S. Gil, G. Férey, P. Couvreur and R. Gref, *Nat. Mater.*, 2010, **9**, 172-178.

View Article Online
DOI: 10.1039/C5TB01412C

19 P. Horcajada, R. Gref, T. Baati, P. K. Allan, G. Maurin, P. Couvreur, G. Férey, R. E. Morris, C. Serre, *Chem. Rev*., 2012, **112**, 1232–1268.
20 M. Meilikhov, S. Furukawa, K. Hirai, R. A. Fischer and S. Kitagawa, *Angew. Chem. Int. Edit.*, 2013, **52**, 341-345.
21 L. E. Kreno, K. Leong, O. K. Farha, M. Allendorf, R. P. Van Duyne and J. T. Hupp, *Chem. Rev.,* 2012, **112**, 1105–1125.
22 S. S. Nagarkar, B. Joarder, A. K. Chaudhari, S. Mukherjee and S. K. Ghosh, *Angew. Chem. Int. Ed,* 2013, **52**, 2881-2885.
23 (a) B. Joarder, A. V. Desai, P. Samanta, S. Mukherjee and S. K. Ghosh, *Chem. Eur. J.* 2015, **21***,* 965 -969; (b) A. V. Desai, P. Samanta, B. Manna and S. K. Ghosh, *Chem. Commun., 2015,* **51***, 6111-6114.*
24 H. Deng, S. Grunder, K. E. Cordova, C. Valente, H. Furukawa, M. Hmadeh, F. Gandara, A. C. Whalley, Z. Liu, S. Asahina, H. Kazumori, M. O'Keeffe, O. Terasaki, J. F. Stoddart, O. M. Yaghi, *Science*, 2012, **336**, 1018-1023.
25 D. Feng, T-F. Liu, J. Su, M. Bosch, Z. Wei, W. Wan, D. Yuan, Y. -P. Chen, X. Wang, K. Wang, X. Lian, Z. –Y. Gu, J. Park, X. Zou, H.-C. Zhou, *Nature Commun*. 2015, **6,** 6979.
26 X. Zhu, H. Zheng, X. Wei, Z. Lin, L. Guo, B. Qiu and G. Chen. *Chem. Commun*., 2013, **49**, 1276-1278.
27 W. Morris, W. E. Briley, E. Auyeung, M. D. Cabezas and C. A. Mirkin, *J. Am. Chem. Soc.*, 2014, **136**, 7261-7264.
28 H.-T. Zhang, J.-W. Zhang, G. Huang, Z.-Y. Du and H.-L. Jiang, *Chem. Commun.*, 2014, **50**, 12069-12072.
29 Y. Chen, S. Han, X. Li, Z. Zhang and S. Ma, *Inorg. Chem*., 2014, **53**, 10006-10008.
30 V. Lykourinou, Y. Chen, X.-S. Wang, L. Meng, T. Hoang, L.-J. Ming, R. L. Musselman and S. Ma, *J. Am. Chem. Soc*., 2011, **133**, 10382-10385.
31 Y. Chen, V. Lykourinou, C. Vetromile, T. Hoang, L.-J. Ming, R. W. Larsen and S. Ma, *J. Am. Chem. Soc.,* 2012, **134**, 13188-1391.
32 Y. Chen, V. Lykourinou, T. Hoang, L-J Ming and S. Ma, *Inorg. Chem.*, 2012, **51**, 9156-9158.
33 W. -L. Liu, N. -S. Yang, Y. -T. Chen, S. Lirio, C. -Y. Wu, C. -H. Lin and H.-Y. Huang, *Chem. Eur. J.*, 2015, **21**, 115-119.
34 S. Jung, Y. Kim, S.-J. Kim, T.-H. Kwon, S. Huh and S. Park, *Chem. Commun.*, 2011, **47**, 2904-2906.
35 W.-L. Liu, S.-H. Lo, B. Singco, C.-C. Yang, H.-Y. Huang and C.-H Lin, *J. Mater. Chem. B*, 2013, **1**, 928-932.
36 W.-L. Liu, C.-Y. Wu, C.-Y. Chen, B. Singco, C.-H. Lin and H.-Y. Huang, *Chem. Eur. J.,* 2014, **20**, 8923-8928.
37 J. Huo, J. Aguilera-Sigalat, S. El-Hankari and D. Bradshaw, *Chem. Sci.*, 2015, **6**, 1938-1943.
38 F. Lyu, Y. Zhang, R. N. Zare, J. Ge and Z. Liu, *Nano Lett*., 2014, **14**, 5761-5765.
39 C. M. Doherty, G. Grenci, R. Riccò, J. I. Mardel, J. Reboul, S. Furukawa, S. Kitagawa, A. J. Hill and P. Falcaro, *Adv. Mater.*, 2013, **25**, 4701-4705.
40 W. Ma, Q. Jiang, P. Yu, L. Yang and L. Mao, *Anal. Chem.*, 2013, **85**, 7550-7557.
41 X. Wang, X. Lu, L. Wu and J. Chen, *Biosens. Bioelectron.*, 2015, **65**, 295-301.
42 S. Patra and N. Munichandraiah, *Langmuir*, 2008, **25**, 1732-1738.
43 A. García Márquez, A. Demessence, A. E. Platero-Prats, D. Heurtaux, P. Horcajada, C. Serre, J.-S. Chang, G. Férey, V. A. de la Peña-O'Shea, C. Boissière, D. Grosso and C. Sanchez, *Eur. J. Inorg. Chem.*, 2012, 5165-5174.
44 A. Dhakshinamoorthy, M. Alvaro, H. Chevreau, P. Horcajada, T. Devic, C. Serre and H. Garcia, *Catal. Sci. Technol.*, 2012, **2**, 324-330.
45 V. Agostoni, T. Chalati, P. Horcajada, H. Willaime, R. Anand, N. Semiramoth, T. Baati, S. Hall, G. Maurin, H. Chacun, K. Bouchemal, C. Martineau, F. Taulelle, P. Couvreur, C. Rogez-Kreuz, P. Clayette, S. Monti, C. Serre and R. Gref, *Adv. Healthcare Mater.*, 2013, **2**, 1630-1637.
46 A. Dhakshinamoorthy, M. Alvaro, Y. K. Hwang, Y.-K. Seo, A. Corma and H. Garcia, *Dalton Trans.*, 2011, **40**, 10719-10724.
47 D. Zhai, B. Liu, Y. Shi, L. Pan, Y. Wang, W. Li, R. Zhang, G. Yu, *ACS Nano*, 2013, **7**, 3540-3546.
48 T. F. Kumosinski and J. J. Unruh, *ACS Symposium Series 576*, 1993, 71-98.
49 X. Chen, H. Xie, J. Kong and J. Deng, *Biosens. Bioelectron.*, 2001, **16**, 115-120.
50 W. Liang and Y. Zhuobin, *Sensors*, 2003, **3**, 544-554.
51 F. R. Shu and G. S. Wilson, *Anal. Chem.*, 1976, **48**, 1679-1686.
52 (a) B. E. P. Swoboda and V. Massey, *J. Biol. Chem.*, 1965, **240**, 2209-2215; (b) Q. H. Gibson, B. E. P. Swoboda and V. Massey, *J. Biol. Chem.*, 1964, **239**, 3927-3934.
53 R. Wilson and A. P. F. Turner, *Biosens. Bioelectron.*, 1992, **7**, 165-185.
54 H.-J. Kim, S. H. Yoon, H. N. Choi, Y.-K. Lyu and W.-Y. Lee, *Bull. Kor. Chem. Soc*, 2006 **27**, 65 - 70.
55 H. N. Choi, M. A. Kim and W.-Y. Lee, *Anal. Chim. Acta*, 2005, **537**, 179-187.
56 L. Yang, X. Ren, F. Tang and L. Zhang, *Biosens.Bioelectron.*, 2009, **25**, 889-895.
57 Z. R. Marand, N. Shahtahmassebi, M. R. Housaindokht, G. H. Rounaghi and I. Razavipanah, *Electroanalysis*, 2014, **26**, 840-848.
58 N. Steunou, C. Mousty, O. Durupthy, C. Roux, G. Laurent, C. Simonnet-Jegat, J. Vigneron, A. Etcheberry, C. Bonhomme, J. Livage and T. Coradin, *J. Mater. Chem.*, 2012, **22**, 15291-15302.
59 Y. Yang, H. Yang, M. Yang, Y. Liu, G. Shen and R. Yu, *Anal. Chim. Acta*, 2004, **525**, 213-220.
60 H. Tang, F. Yan, Q. Tai and H. L. W. Chan, *Biosens. Bioelectron.*, 2010, **25**, 1646-1651.
61 J. R. Anusha, H.-J. Kim, A. T. Fleming, S. J. Das, K.-H. Yu, B. C. Kim and C. J. Raj, *Sens. Actuat. B: Chem.*, 2014, **202**, 827-833.
62 I. Ben Assaker, Ph.D. Thesis, Université d'Evry, France, 2009.
63 J.-W. Zhang, H.-T. Zhang, Z.-Y. Du, X. Wang, S.-H. Yu and H.-L. Jiang, *Chem. Commun.*, 2014, **50**, 1092-1094.
64 L. Ai, L. Li, C. Zhang, J. Fu, and J. Jiang, *Chem. Eur. J.* , 2013, **19**, 15105-15108.
65 Y. L. Liu, X. J. Zhao, X. X. Yang and Y. F. Li, *Analyst*, 2013, **138**, 4526-4531.

View Article Online
DOI: 10.1039/C5TB01412C

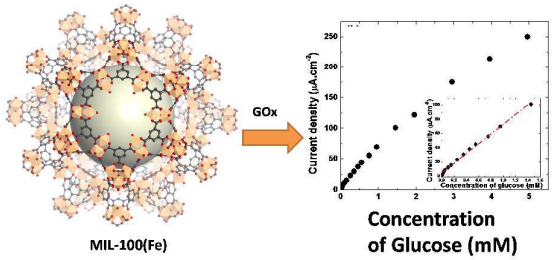

The mesoporous iron(III) trimesate MIL-100 (Fe) based biosensor presents very interesting electrocatalytic performances for glucose detection.